

Dependence of the physical properties of $Nd_{0.5}Ca_{0.5}MnO_{3+\delta}$ on the oxydation state of Mn .

Carlos Frontera and José Luis García-Muñoz

Institut de Ciència de Materials de Barcelona, CSIC, Campus de la UAB, E-08193 Bellaterra, Spain.

Anna Llobet

Laboratoire Louis Néel, 25 avenue des Martyrs, Polygone CNRS BP 166, 38042 Grenoble CEDEX 09, France.

Clemens Ritter

Institute Laue Lagevin, 6, rue Jules Horowitz, BP 156, 38042 Grenoble-Cedex 9, France.

José Antonio Alonso

Instituto de Ciencia de Materiales de Madrid, CSIC, Cantoblanco, 28049 Madrid, Spain.

Juan Rodríguez-Carvajal

Laboratoire Léon Brillouin, CEA-CNRS, Centre d'Etude de Saclay, 91191 Gif sur Yvette Cedex, France.

(November 19, 2018)

We present a comparative study of the magnetic, transport and structural properties of $Nd_{0.5}Ca_{0.5}MnO_{3+\delta}$ [$\delta = 0.02(1)$ and $0.04(1)$]. We have found significant differences between the low temperature magnetic orders and the magnetization curves below $T_{CO} \approx 250K$ of the two samples. In particular one component of the magnetic moment presents a ferromagnetic coupling between the (0 0 1) planes ($Pbnm$ setting) deviating the angle between neighboring Mn ions from 180° (perfect CE order) to 150° [$\delta = 0.02(1)$] and 130° [$\delta = 0.04(1)$]. These results imply a remarkable δ dependence which is discussed in the light of a non-random spatial distribution of defects in the perfect charge order scheme.

A considerable research effort concerning the charge order (CO) phenomenon in doped manganites ($Ln_{1-x}A_xMnO_3$ with $Ln =$ rare earth and $A =$ alkaline earth) has been made during the last years. Ingredients such as Coulomb repulsion, the effect of Jahn-Teller distortion on the e_g energy levels and lattice distortions play an important role on the stability of the CO state. This state is usually accompanied by a real space ordering of the orbitals occupied by the e_g electrons. When this orbital order (OO) occurs, the Mn - O - Mn superexchange interactions are FM if a half-filled $d_{3r^2-r^2}$ ($r_i = x, y$ or z) and an empty e_g orbitals are involved and antiferromagnetic (AFM) if the involved ones are two t_{2g} orbitals.^{2,1} This makes the magnetic behavior to be strongly dependent on (i) the mean valence state of the Mn ions (or, equivalently, on the density of e_g electrons) and (ii) the real space OO. When the formal ratio $\frac{Mn^{+4}}{Mn^{+3}}$ ions is 1, and for a rich variety of rare earths the low temperature magnetic structure found is the CE². This structure is usually explained as resulting from a well established CO and OO.^{1,2} Some previous works have been devoted to study how the off-stoichiometry of the $\frac{Mn^{+4}}{Mn^{+3}} = 1$ ratio affects the CO.³⁻⁷ One interesting effect is the variation in the CO modulation wave vector [$\mathbf{Q} = \frac{2\pi}{a}(0 \ 1/2 - \alpha \ 0)$ in the $Pbnm$ setting] that different annealing conditions produce, for example, in $Pr_{0.5}Ca_{0.5}MnO_3$ and in $Sm_{0.5}Ca_{0.5}MnO_3$.⁵ Incom-

mensurability of the CO in $La_{0.5}Ca_{0.5}MnO_3$ have also been reported in the temperature range of the structural transformation, but it disappears at lower temperature.⁸ Barnabé *et al.* (Ref. 5) argue that in an under-doped sample (presenting CO) the extra e_g electrons are randomly placed in the Mn positions leaving the CO commensurated ($\alpha = 0$), but the extra Mn^{+4} ions of an over-doped sample introduce incommensurability in the CO structure ($\alpha > 0$) even when the excess of Mn^{+4} is very small. Using electron diffraction data, Barnabé *et al.* conclude that the extra Mn^{+4} ions form ordered (0 1 0) planes. Such an incommensurability of an over-doped sample has been also reported by Chen *et al.* in Ref. 6.

In this brief report we present the effects of changing the oxydation state of Mn in $Nd_{0.5}Ca_{0.5}MnO_{3+\delta}$. The notation we use here is convenient from the point of view of the chemical formulation, but the actual structural defects are not interstitial oxygens, they should correspond to cation vacancies. This study is based on the comparison of the structural, magnetic and transport properties. The main changes correspond to the magnetic structure. Its evolution with δ indicates that the extra holes due to δ are not randomly distributed.

Two different polycrystalline samples have been sintered by standard solid state reaction by mixing high purity powders of $CaCO_3$, Mn_2O_3 and Nd_2O_3 in appropriate ratios for the nominal composition $Nd_{1/2}Ca_{1/2}MnO_3$. After some intermediate treatments,

the two samples were pressed into pellets, fired and ground again for several times. For the first sample (air sample) the firings were done at 1450°C in air followed by a rapid quench to RT ($-500^{\circ}\text{C}/\text{hour}$). For the second sample (O_2 sample) the firings were done at 1400°C in an atmosphere of flowing O_2 and the final one was followed by a slow cooling to RT ($-50^{\circ}\text{C}/\text{hour}$). X-ray powder diffraction confirmed that both samples are well crystallized in a single phase. Agreeing with the synthesis conditions, thermogravimetric analysis (TGA), used to determine the oxygen content of the samples ($\text{Nd}_{0.5}\text{Ca}_{0.5}\text{MnO}_{3+\delta}$), evidenced a larger content of oxygen in the O_2 ($\delta = 0.04(1)$, $\text{Mn}^{+4} = 58(2)\%$) than in air sample ($\delta = 0.02(1)$, $\text{Mn}^{+4} = 54(2)\%$). Neutron diffraction (ND) patterns of the air sample were collected at the Institute Laue Langevin (Grenoble) using D2B ($\lambda = 1.594\text{\AA}$) and D1B ($\lambda = 2.52\text{\AA}$) diffractometers. ND patterns of the O_2 sample were collected at the Laboratoire Leon Brillouin (Paris) using 3T2 ($\lambda = 1.227\text{\AA}$) and G4.2 ($\lambda = 2.426\text{\AA}$) diffractometers. For both samples, ND patterns were collected for several temperatures in the range 1.5K to room temperature (RT). They were analyzed by the Rietveld method using the program FULLPROF.⁹ Resistivity was measured by the four-probe method using a commercial PPMS (Quantum Design). Magnetization measurements have been carried out using a commercial SQUID (Quantum Design).

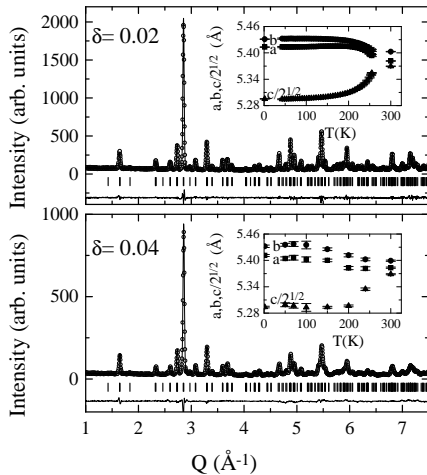


FIG. 1. Refined ND patterns at RT of both samples (D2B for $\text{Nd}_{0.5}\text{Ca}_{0.5}\text{MnO}_{3.02(1)}$ and 3T2 for $\text{Nd}_{0.5}\text{Ca}_{0.5}\text{MnO}_{3.04(1)}$). Inset: evolution with temperature of the lattice parameter for $\text{Nd}_{0.5}\text{Ca}_{0.5}\text{MnO}_{3.02(1)}$ (using D1B) and $\text{Nd}_{0.5}\text{Ca}_{0.5}\text{MnO}_{3.04(1)}$ (using G4.2).

Figure 1 shows the high-resolution ND patterns, collected at RT, refined using an average $Pbnm$ structure. The refined lattice parameters, Mn-O bond lengths and Mn-O-Mn bond angles are listed in Tab. I for comparison. There is a good agreement between the structural parameters obtained for $\text{Nd}_{0.5}\text{Ca}_{0.5}\text{MnO}_{3.02(1)}$ with those for $\text{Nd}_{0.5}\text{Ca}_{0.5}\text{MnO}_{3.04(1)}$ and with those pre-

viously reported for $\text{Nd}_{0.5}\text{Ca}_{0.5}\text{MnO}_3$.¹⁰ The lattice parameters show a negligible compression of the c -axis. The MnO_6 octahedra are very regular and without any appreciable apical compression. In order to check the mean oxidation state of the Mn ions using ND data, we refined the occupation factors of Nd , Ca and Mn ions assuming that no interstitial oxygens are present (that is, fixing the oxygen stoichiometry to 3). It is known that any excess of oxygen in perovskites always corresponds to the presence of cation vacancies since there is no space left in the perovskite structure to allocate interstitial oxygens. We observed no improvement of the refinement factors and no significant differences between the nominal composition and the refined values: $\text{Nd}_{0.502(8)}\text{Ca}_{0.492(8)}\text{Mn}_{1.001(9)}\text{O}_3$ for the air sample $\text{Nd}_{0.496(8)}\text{Ca}_{0.492(8)}\text{Mn}_{0.992(8)}\text{O}_3$ for the O_2 sample.

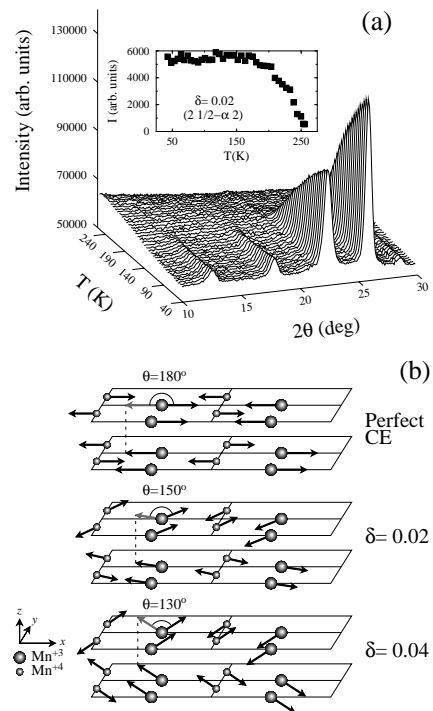


FIG. 2. (a) Low angle region of the collected ND patterns showing the onset of the AFM order. Inset: Integrated intensity of the $(2\ 1/2-\alpha\ 2)$ superlattice peak showing the CO/OO transition. Both correspond to $\text{Nd}_{0.5}\text{Ca}_{0.5}\text{MnO}_{3.02(1)}$ data collected at D1B diffractometer. (b) Scheme of the magnetic structures obtained for $\text{Nd}_{0.5}\text{Ca}_{0.5}\text{MnO}_{3.02(1)}$ (middle) and $\text{Nd}_{0.5}\text{Ca}_{0.5}\text{MnO}_{3.04(1)}$ (bottom) compared to that of the perfect CE-type order (top). The arrows in grey of the upper planes correspond to the translation of the magnetic moment of the Mn placed just below, in order to visualize the angle between the two magnetic moments.

ND patterns of both samples present superlattice peaks below $T_{CO} \approx 250\text{K}$, attributed to the development of the CO/OO state. A small incommensurability of the charge order can be appreciated through the position of the $(2\ 1/2-\alpha\ 2)$ peak for the $\text{Nd}_{0.5}\text{Ca}_{0.5}\text{MnO}_{3.04(1)}$ sam-

ple [$\alpha = 0.03(1)$] but not, within the resolution of our ND data, for the $Nd_{0.5}Ca_{0.5}MnO_{3.02(1)}$ sample ($\alpha \approx 0$). The inset of Fig. 2(a) shows the growth of the $(2\ 1/2 - \alpha\ 2)$ peak found for $Nd_{0.5}Ca_{0.5}MnO_{3.02(1)}$. Its integrated intensity relative to that of the $(0\ 2\ 2)$, $(2\ 0\ 2)$ positions is, at low temperature, $I_{(2\ 1/2 - \alpha\ 2)}/I_{(0\ 2\ 2), (2\ 0\ 2)} = 7.4 \cdot 10^{-3}$ for $Nd_{0.5}Ca_{0.5}MnO_{3.02(1)}$ and $7.1 \cdot 10^{-3}$ for $Nd_{0.5}Ca_{0.5}MnO_{3.04(1)}$, indicating a very similar degree of long range ordering in both samples. The effect on the lattice parameters of the CO/OO is shown in the insets of Fig. 1. The strong compression of the c lattice parameter is due to the localization of the e_g electrons in $d_{3x^2-r^2}$ or $d_{3y^2-r^2}$ orbitals contained in the $(0\ 0\ 1)$ planes. The low temperature ND patterns have been refined using the $Pbnm$ description of the single cell. The obtained lattice parameters, $Mn-O$ bond distances and $Mn-O-Mn$ bond angles are listed in Tab. I. The aforementioned in-plane localization of the e_g electrons causes an apical compression of the MnO_6 octahedra that can be quantified through the parameter $\epsilon_d = \left| 1 - \frac{d_{Mn-O1}}{\langle d_{Mn-O2} \rangle} \right| \times 10^4$. ϵ_d is, at low temperature, about four times larger than at RT for both samples. $La_{1/2}Ca_{1/2}MnO_3$ ($\epsilon_d = 205$)¹ and $Nd_{1/2}Sr_{1/2}MnO_3$ ($\epsilon_d = 215$)¹¹, both presenting CO and a CE-type magnetic structure, present an apical compression comparable to $Nd_{0.5}Ca_{0.5}MnO_{3.02(1)}$ ($\epsilon_d = 217$). A little lower value is found for $Nd_{0.5}Ca_{0.5}MnO_{3.04(1)}$ ($\epsilon_d = 192$), reflecting the partial lack of e_g electrons.

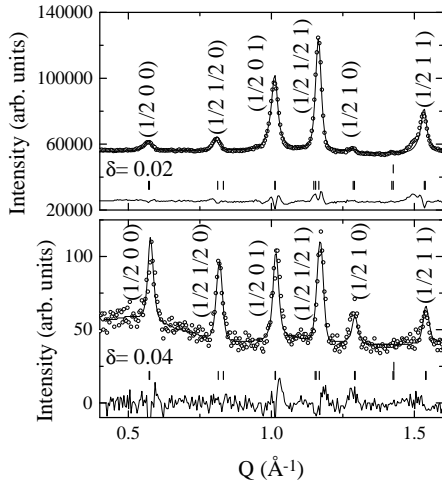


FIG. 3. Detail of the low temperature refined patterns showing the low angle region with the most intense magnetic peaks. $\lambda = 2.52\text{\AA}$ (D1B) has been used for $Nd_{0.5}Ca_{0.5}MnO_{3.02(1)}$ and $\lambda = 2.426\text{\AA}$ (G4.2) for $Nd_{0.5}Ca_{0.5}MnO_{3.04(1)}$.

Figure 2(a) shows the temperature evolution of the low angle region of the ND patterns of $Nd_{0.5}Ca_{0.5}MnO_{3.02(1)}$. The apparition of magnetic reflections is observed to occur at $T_{N1} = 165\text{K}$ [$Nd_{0.5}Ca_{0.5}MnO_{3.02(1)}$] and $T_{N2} = 150\text{K}$ [$Nd_{0.5}Ca_{0.5}MnO_{3.04(1)}$]. The low angle regions of the refined ND patterns at low temperature are plotted in

Fig. 3 for both samples. The magnetic peaks have been indexed on the basis of the $Pbnm$ setting. In both samples, there are two families of magnetic peaks displaying $(h\ k\ l)$ Miller indices with h half integer and k both integer or half integer. The first family of peaks has $l = \text{odd}$ [$(1/2\ 0\ 1)$, $(1/2\ 1/2\ 1)$, ...] and is associated to the CE-type AFM structure.^{2,1} The second family of peaks has $l = \text{even}$ [$(1/2\ 0\ 0)$, $(1/2\ 1/2\ 0)$, ...] and is usually associated to the *pseudo CE-type* AFM structure.¹² These two families of peaks are also present in $Nd_{0.45}Ca_{0.55}MnO_3$.¹³ We have obtained good fits to the ND patterns assuming that the components of the magnetic moment contained in the $(0\ 0\ 1)$ planes (m_x and m_y) present a CE-type order structure, while the component of the magnetic moment in the $[0\ 0\ 1]$ direction (m_z) presents a *pseudo CE-type* AFM order. The obtained magnetic structures are described in Tab. II and schematically plotted in Fig. 2(b). In both cases the ordered moments are well below the expected values for perfectly ordered moments. The effect of the considered out-of-plane component of the magnetic moment can be interpreted as a deviation from the perfect value (180°) of the angles formed by the magnetic moments in neighboring $(0\ 0\ 1)$ planes [e.g. between the magnetic moments of the Mn^{+3} ions in positions $(\frac{1}{4}, \frac{1}{2}, 0)$ and $(\frac{1}{4}, \frac{1}{2}, \frac{1}{2})$ of Tab. II as is schematically depicted in Fig. 2(b)] that is about 30° in $Nd_{0.5}Ca_{0.5}MnO_{3.02(1)}$ and 50° in $Nd_{0.5}Ca_{0.5}MnO_{3.04(1)}$.

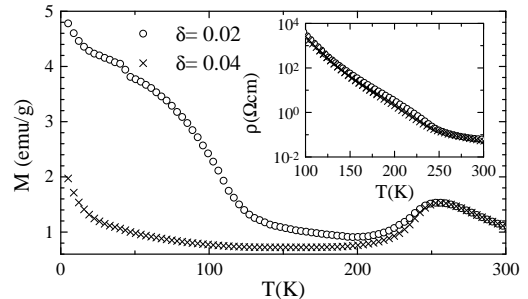


FIG. 4. Temperature evolution of the magnetization $M(T)$ (applied field $0.5T$) and $\rho(T)$ (inset) for both $Nd_{0.5}Ca_{0.5}MnO_{3.02(1)}$ and $Nd_{0.5}Ca_{0.5}MnO_{3.04(1)}$.

The magnetization [$M(T)$] and resistivity [$\rho(T)$] curves are shown in Fig. 4 and its inset respectively. The CO transition can be well appreciated as a sudden increase in the $\rho(T)$ curves, caused by the localization of the charges, and as a local maximum in the $M(T)$ curves. This local maximum is due to the transition from the FM $Mn-Mn$ correlations above T_{CO} (double-exchange) to the AFM $Mn-Mn$ correlations below T_{CO} ($Mn-O-Mn$ superexchange). There is scarcely any variance in $\rho(T)$ from one sample to the other. In this sense, the magnetization curves clearly show two regimes: above T_{CO} both curves are almost identical, but below this point the curves systematically start to come away.

The results presented in the previous paragraphs show

that the two samples are indeed very similar: the different oxydation state of the Mn does not significantly change the structure, the transport and the magnetic properties of the compound above T_{CO} . Consequently, the differences observed at lower temperatures cannot be attributed to intrinsic differences in the structure due to the different concentration of cation vacancies.

In contrast with the behavior above T_{CO} , substantial discrepancies in the $M(T)$ curves start at this temperature, just when the $Mn-O-Mn$ superexchange interactions are dominated by the real space location of the e_g electrons. This indicates that the difference in the magnetic behavior of the samples is driven by the defects introduced by the lack of e_g electrons in the OO state. The different density of carriers causes differences in the real space distribution of $Mn-O-Mn$ superexchange interactions giving rise to a dissimilar $M(T)$ evolution. The presence of defects in the OO structure gives rise to frustrated magnetic coupling and, hence, differences between the magnetic structure and the perfect CE-type. To be emphasized is that such great changes in the obtained magnetic order and in the $M(T)$ are hard to explain in the scenario of a random location of the holes among Mn positions. The last will simply lead to a CE structure with disorder. Consequently, a certain spatial grouping of the defects may enhance their effects and also cause the small incommensurability of the CO.

Of special interest is to determine if the two families of magnetic peaks are sustained by the same structural lattice or they correspond to two slightly different lattices. In $Nd_{0.5}Sr_{0.5}MnO_3$, the coexistence of an A-type and a CE-type AFM phases below the CO transition, supported by different crystallographic cells, has been attributed to inhomogeneities in the cation distribution.¹⁴ In the present case (for both samples) the two families of magnetic peaks can be very well reproduced using the same lattice parameters and appear at the same temperature [see Fig. 2(a)]. Within our resolution, a single set of cell parameters allows a proper indexation of all the magnetic intensities (see Fig. 3).

In summary, off-stoichiometric samples of $Nd_{0.5}Ca_{0.5}MnO_{3.02(1)}$ [$\%Mn^{+4} = 54(2)$] and $Nd_{0.5}Ca_{0.5}MnO_{3.04(1)}$ [$\%Mn^{+4} = 58(2)$] samples have been investigated in comparison with the stoichiometric $Nd_{0.5}Ca_{0.5}MnO_3$. The same structural features and macroscopic behavior are observed above T_{CO} . A detailed ND study reveals pronounced influence of the different, but very similar, oxydation state of Mn upon the magnetic long range ordering. The intensities of the magnetic ($h/2$ $k/2$ 0) peaks (absent in the CE-type order) increase significantly with the value of δ . As a result the angle formed by the spins of successive MnO_2 (0 0 1) planes change from $\theta = 180^\circ$ for $\delta = 0$ to $\theta = 130^\circ$ for $\delta = 0.04$. These remarkable changes in the magnetic structure are unusually important compared to the effects of a small off-stoichiometry in most of the transition metal oxides. They indicate, in connection with the in-

commensurability of the CO detected for the $\delta = 0.04(1)$ sample, that the extra holes are not randomly placed in the Mn positions but they form spatial sub-structures.

This work has been done with financial support from the CICyT (MAT97-0669) MEC (PB97-1175) and Generalitat de Catalunya (GRQ95-8029). A.L. acknowledges financial support from the Oxide Spin Electronics Network (EU TMR) program. The ILL and LLB are acknowledged for making available the beam time.

-
- ¹ P.G. Radaelli, D.E. Cox, M. Marezio, and S.-W. Cheong, Phys. Rev. B **55**, 3015 (1997).
 - ² E.O. Wollan and W.C. Koehler, Phys. Rev. **100**, 545 (1955). J.B. Goodenough, Phys. Rev. **100**, 564 (1955).
 - ³ M. Roy, J.F. Mitchell, A.P. Ramirez and P. Schiffer, Phys. Rev. B **58**, 5185 (1998).
 - ⁴ Y. Tomioka, A. Asamitsu, H. Kuwahara, Y. Moritomo and Y. Tokura, Phys. Rev. B **53**, R1689 (1996).
 - ⁵ A. Barnabé, M. Hervieu, C. Martin, A. Maignan, and B. Raveau, J. of Appl. Phys. **84**, 5506 (1998).
 - ⁶ C.H. Chen, S. Mori, and S-W. Cheong, Phys. Rev. Lett. **83**, 4792 (1999).
 - ⁷ O. Richard, W. Schuddinck, G. Van Tendeloo, F. Millange, M. Hervieu, V. Caignaert, and B. Raveau, Acta Cryst. **A55**, 704 (1999).
 - ⁸ C.H. Chen and S-W. Cheong, Phys. Rev. Lett. **76**, 4042 (1996).
 - ⁹ J. Rodríguez-Carvajal, Physica B **192** (1993) 55.
 - ¹⁰ P.M. Woodward, T. Vogt, D.E. Cox, A. Arulraj, C.N.R. Rao, P. Karen, and A.K. Cheetham, Chem. Mater. **10**, 3652 (1998).
 - ¹¹ R.Kajimoto, H. Kawano, H. Kurwahara, Y. Tokura, K. Ohoyama and M. Ohashi, Phys. Rev. B **60**, 9506 (1999).
 - ¹² AFM (0 0 1) planes coupled ferromagnetically [see Z. Jiráček, S. Krupička, Z. Šimša, M. Dlouhá, and S. Vratislav, J. Magn. Magn. Mater. **53**, 153 (1985)].
 - ¹³ W.-H. Li, S.Y. Wu, K.C. Lee, J.W. Lynn, R.S. Liu, J.B. Wu, and C.Y. Huang, J. App. Phys. **85**, 5588 (1999).
 - ¹⁴ P.M. Woodward, D.E. Cox, T. Vogt, C.N.R. Rao and A.K. Cheetham, Chem. Mater. **11**, 3528 (1999).

TABLE I. Refined structural parameters of $Nd_{0.5}Ca_{0.5}MnO_{3+\delta}$ at room and low temperature. Parameter ϵ_d is defined in the text. O1 stands for apical and O2 for basal oxygens.

	$\delta = 0.02(1)$ (D2B)		$\delta = 0.04(1)$ (3T2)	
	4K	RT	1.5K	RT
a (Å)	5.4133(6)	5.3821(4)	5.4055(7)	5.3771(6)
b (Å)	5.4326(6)	5.4038(4)	5.4259(7)	5.4010(6)
c (Å)	7.4927(7)	7.5923(4)	7.4807(8)	7.5874(8)
V (Å ³)	220.35	220.81	219.40	220.35
$\sqrt{2}c/(a+b)$	0.977	0.995	0.977	0.996
$\langle d_{Mn-O1} \rangle$	1.9106(9)	1.9354(6)	1.9142(9)	1.933(1)
$\langle d_{Mn-O2} \rangle$	1.953(3)	1.946(2)	1.952(4)	1.945(4)
$\langle d_{Mn-O} \rangle$	1.939(2)	1.942(2)	1.939(3)	1.941(3)
ϵ_d	217(14)	52(9)	192(18)	59(15)
$\theta_{Mn-O1-Mn}(deg.)$	157.3(1)	157.4(1)	155.5(1)	157.8(1)
$\theta_{Mn-O2-Mn}(deg.)$	158.1(1)	157.0(1)	157.9(2)	156.9(2)
$\langle \theta_{Mn-O-Mn} \rangle (deg.)$	157.8(1)	157.2(1)	157.8(2)	157.2(2)
χ^2	3.6	2.3	3.8	2.8
$R_N(\%)$	8.0	4.8	8.5	8.3

TABLE II. Magnetic structures obtained at low temperature for $Nd_{0.5}Ca_{0.5}MnO_{3.02(1)}$ and $Nd_{0.5}Ca_{0.5}MnO_{3.04(1)}$. The atomic positions are referred to the magnetic lattice ($2a \times 2b \times c$).

	Position	$Nd_{0.5}Ca_{0.5}MnO_{3.02(1)}$ (D1B) ($R_{mag} = 8\%$)				$Nd_{0.5}Ca_{0.5}MnO_{3.04(1)}$ (G4.2) ($R_{mag} = 7\%$)			
		$m_x(\mu_B)$	$m_y(\mu_B)$	$m_z(\mu_B)$	$m_T(\mu_B)$	$m_x(\mu_B)$	$m_y(\mu_B)$	$m_z(\mu_B)$	$m_T(\mu_B)$
Mn^{+3}	$(\frac{1}{4}, 0, 0); (\frac{1}{4}, \frac{1}{2}, 0)$	1.9(1)	1.9(1)	0.7(2)	2.8(2)	2.5(2)	0	1.5(1)	3.0(2)
	$(\frac{1}{4}, 0, \frac{1}{2}); (\frac{1}{4}, \frac{1}{2}, \frac{1}{2})$	-1.9(1)	-1.9(1)	0.7(2)		-2.5(2)	0	1.5(1)	
	$(\frac{3}{4}, 0, 0); (\frac{3}{4}, \frac{1}{2}, 0)$	-1.9(1)	-1.9(1)	-0.7(2)		-2.5(2)	0	-1.5(1)	
	$(\frac{3}{4}, 0, \frac{1}{2}); (\frac{3}{4}, \frac{1}{2}, \frac{1}{2})$	1.9(1)	1.9(1)	-0.7(2)		2.5(2)	0	-1.5(1)	
Mn^{+4}	$(0, \frac{1}{4}, 0); (\frac{1}{2}, \frac{3}{4}, 0)$	1.7(1)	1.7(1)	0.7(2)	2.5(2)	1.9(2)	0	1.3(1)	2.5(1)
	$(0, \frac{1}{4}, \frac{1}{2}); (\frac{1}{2}, \frac{3}{4}, \frac{1}{2})$	-1.7(1)	-1.7(1)	0.7(2)		-1.9(2)	0	1.3(1)	
	$(0, \frac{3}{4}, 0); (\frac{1}{2}, \frac{1}{4}, 0)$	-1.7(1)	-1.7(1)	-0.7(2)		-1.9(2)	0	-1.3(1)	
	$(0, \frac{3}{4}, \frac{1}{2}); (\frac{1}{2}, \frac{1}{4}, \frac{1}{2})$	1.7(1)	1.7(1)	-0.7(2)		1.9(2)	0	-1.3(1)	